ACS OMEGA

Open Access



http://pubs.acs.org/journal/acsodf

Article

# Preparation and Characteristics of Building Dust Suppressants with Strong Resistance to Harsh Environments

Hao Ding, Zhian Huang, Shijie Peng,* Hongsheng Wang,* Jinyang Li, Ruixiang Wang, Yinghua Zhang,* and Pengfei Wang

Cite This: *ACS Omega* 2024, 9, 3746−3757

Read Online

ACCESS | Metrics & More | Article Recommendations

**ABSTRACT:** Most dust suppressants used for buildings currently lack sufficient resistance to harsh conditions, such as high temperatures and wind erosion. To solve this problem, it is necessary to develop a new type of dust suppressant. In this study, the guar gum molecule was chemically modified to remove the active hydroxyl group in order to significantly improve the stability and adhesion of guar gum. Eventually, a composite dust suppressant was synthesized by incorporating a surfactant and an absorbent agent into modified guar gum. The functional groups of the reaction products were analyzed via infrared experiments, thus confirming the success of the modification. Wind erosion resistance and scanning electron microscopy experiments confirmed the improved bonding capabilities of the composite dust suppressant with dust particles. In experiments on wind erosion resistance, the dust fixation rate exceeded 50% after the application of the composite dust suppressant. The results of the thermogravimetric tests showed that the maximum mass loss rate of the samples with modified guar gum dust suppressants was 6.0% and 28% lower than those of the samples with unmodified guar gum dust suppressants and water, respectively. Furthermore, the tests conducted on pH value and corrosion resistance indicated that the pH value of this dust suppressant was comparable to that of tap water and demonstrated a similar rate of metal corrosion. The practical significance of this study is to improve the dust suppressant used in buildings, to improve the performance of dust suppressant and resistance to harsh environment, and to help to continuously improve the health of personnel and environmental protection during construction. The practical significance of this study is to improve the dust suppressant used in buildings, to improve the performance of dust suppressant and resistance to harsh environments, and to help to continuously improve the health of personnel and environmental protection during construction, which has positive practical significance for the building industry and related fields.

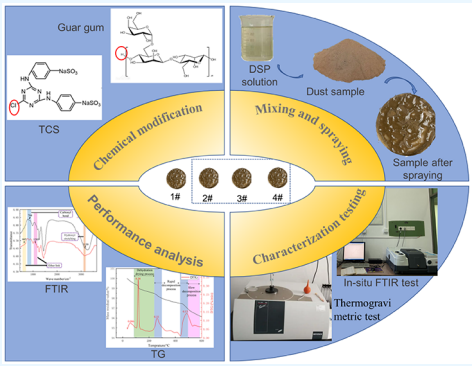


## 1. INTRODUCTION

With the rapid development of the economy, environmental protection has become more urgent and important. Economic development is usually accompanied by the process of industrialization and urbanization, in which the large consumption of resources and the large amount of pollutants generated will have pressure and impact on the environment.[1] Therefore, protecting the environment has become one of the important goals through which to achieve sustainable development. The impacts of building construction processes on the environment have become a hotspot of research. Initial studies focused only on the impact of construction activities on groundwater[2,3] and the neighboring soil environment.[4,5] However, with the increasing awareness of environmental protection, the dust pollution caused by construction is gradually being recognized by more and more people.[6] A complete construction process generates a large amount of dust, mainly fine particles, with particles less than 10 $\mu$m in diameter accounting for about 90% of the total emissions.[7] The generation of these fine particles not only significantly reduces the quality of the surrounding air but can also cause damage to equipment and shorten its service life.[8,9] Moreover, these particles have the potential to enter the human body through inhalation, thereby disrupting gas exchange within the lungs and increasing the transmission of respiratory diseases.[10] Therefore, there is an imperative requirement for swift and efficient control measures to address the growing problem of dust pollution from construction sites.

At present, the traditional methods of dust suppression mainly include two kinds of dust suppression: water sprinkling and the dust prevention net.[11] The former works for only a

Received: October 5, 2023
Revised: December 9, 2023
Accepted: December 14, 2023
Published: January 8, 2024

short time after spraying, and it is difficult to resist various harsh environmental conditions. In a high-temperature environment, rapid water evaporation requires the frequent sprinkling of a large volume of water to control dust levels. This not only wastes water, but also leads to ineffective dust suppression and significant cost.[12,13] Dust net dust suppression methods have the shortcomings of low dust suppression efficiency, material recycling difficulties, high cost, etc. Moreover, the natural environment's acidic substances might corrode the dust net, leading to secondary pollution.[14,15] With the countries' emphasis on environmental protection, these two traditional methods of dust suppression are no longer able to meet the current demand for dust control. As a result, they have gradually become outdated and have been replaced with new methods of dust suppression.

As scholars continue to explore, chemical dust suppressants (DSPs), due to their excellent dust suppression performance, convenience, and other advantages, have gradually attracted people's attention. The development of DSPs for dust suppression work has initiated a new research direction. According to their mechanism of action, DSPs can be divided into the following four major categories: bonding-agent-based DSPs, wetting-agent-based DSPs, cohesive DSPs based on moisture-absorbing materials such as inorganic salts, and composite DSPs with a variety of effects. For example, Pokonova et al.[16] developed a bonded DSP product, consisting of petroleum residue and an emulsifier, that effectively bonded small dust particles together. The application results were positive. Shi et al.[17] developed a cohesive-type DSP and tested the effects of various inorganic salts and resins on the control of dust on transportation roads, among which lignosulfonate had an excellent effect. The results of field experiments showed that this DSP product could effectively reduce dust pollution in the dry season. Amato et al.[18] used polyoxyethylene and polyethylene glycol nonionic surfactants to prepare a wetting DSP, which can effectively reduce the surface tension of the solution and improve the wettability of hydrophobic coal dust. Parsakhoo et al.[19] prepared an environmentally friendly DSP via methods of chemical polymerization using sugar cane molasses and bentonite as raw materials. Dust emission from forest roads was monitored for a long period of time, and the results showed that dust emission decreased gradually with an increase in DSP dosage. The type and dosage of DSPs had an important effect on the dust suppression effect. Orszulik et al.[20] found that the addition of preparations containing active substances effectively inhibited coal dust pollution and reduced the surface tension of water. After use, the total dust in mine air was reduced by 50% and respirable dust was reduced by 40%. Xu et al.[21] used triethanolamine and Tritonx-100 to balance a water-absorbing inorganic salt DSP, thereby successfully reducing its corrosiveness while maintaining its properties. Medeiros et al.[22] have developed a sophisticated and effective chemical DSP using glycerine byproducts that provides impressive dust suppression and is cost-effective.

Although chemical DSPs are increasingly used in dust suppression applications, most existing options still have several shortcomings, such as poor solubility, limited application, or cumbersome application steps, as well as frequent application and a short duration of action.[23,24] Little attention has been given to researching DSPs for the harsh environment of continued resistance. The application of polymer organic synthetic materials and other components in DSPs under persistent, high-temperature conditions may easily decompose and produce toxic substances. It negatively impacts the structure of the surrounding soil, ecological environment, and production with secondary pollution.[25,26]

Due to the serious issue of dust pollution, it is imperative to develop a DSP product with high effectiveness, durability in harsh environments, and prolonged action. This suppressant must fulfill the need for immediate dust control while ensuring it does not fail shortly in tough environments. In this research, guar gum (GG) was selected as the binder of the composite DSP. Guar gum is a natural galactomannan gum, and it is rich in reserves, can be obtained from a wide range of sources, and is nontoxic, nonharmful, naturally degradable, and renewable. In some industrial production applications, guar gum can be said to be the most ideal binder.[27,28] However, the research and development of DSPs also reveals outcomes such as a low dissolution rate, high insoluble matter content, and microbial and high temperature degradation.[29,30] Taunk[31] plotted the TGA and DTA curves of guar gum. The results showed that the thermal stability of guar gum aqueous solution is poor, and with high temperature heating for a period of time, it will lose viscosity. As a natural polymer, guar gum is also easily decomposed by enzymes and bacteria, and it cannot be stored for a long time.[32] These shortcomings make the application of guar gum greatly restricted. Therefore, there is a need to change their physicochemical properties so that they can be used in a wide range of applications.

The surfactant selected for this research is rhamnolipid (CAS), which is an anionic biosurfactant produced by microorganisms. This substance possesses favorable chemical and biological attributes. It effectively lowers the surface tension and facilitates the wetting of dust. Moreover, CAS exhibits remarkable stability even under extreme conditions of temperature, pH, and salinity. Importantly, it is nontoxic and poses no hazards.

The hygroscopic agent selected in this study was polyethylene glycol (PEG). PEG has excellent absorbency, moisture retention, and thermal stability, making it highly common in various metal and food processing industries. Not only can it be used as a water retaining agent but it can also improve the thermal stability of compound DSP.

In this study, GG was selected as a natural biopolymer binder, and an active modifier was added under specific experimental conditions to make it rich in hydrophilic groups, such as amino groups, via methods of chemical modification, and hydroxyl groups were eliminated at the same time to reduce the molecular activity of guar gum. In this way, modified guar gum with good water solubility, high-temperature resistance to evaporation, and low molecular activity (GGTCS) was prepared. By incorporation of the surfactant CAS and the hygroscopic agent PEG, a novel multifunctional DSP was created that integrates wetting, bonding, and absorption. The suppressant offers outstanding dust suppression effects and adaptability to harsh environments, which present novel ideas for further multifunctional DSP development.

## 2. MATERIALS AND METHODS

This section analyzes the comprehensive dust suppression performance of GGTCS composite DSP through a Fourier transform infrared experiment, scanning electron microscopy test, thermogravimetric experiment, wind erosion resistance test, and environmental hazard test.



https://doi.org/10.1021/acsomega.3c07734
ACS Omega 2024, 9, 3746−3757

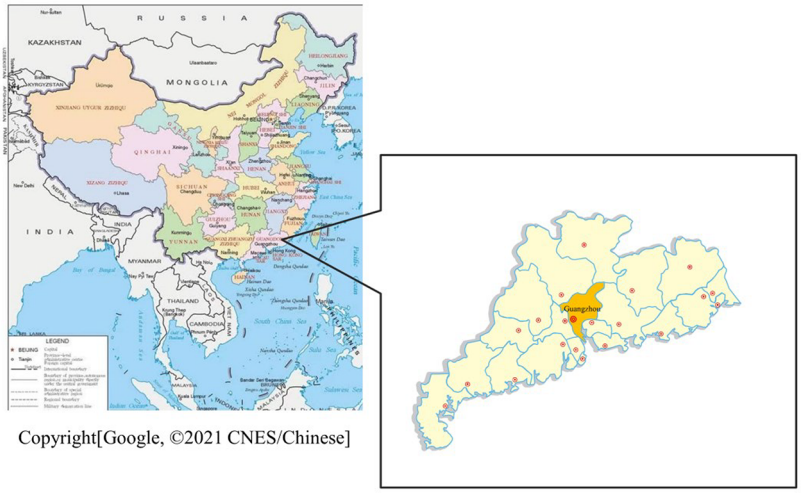


**Figure 1.** Dust sampling location.

**2.1. Dust Samples.** In this study, dust samples were obtained from a construction site in Guangzhou, China. The dust samples were collected using an IFC-2 dust sampler in a building field according to the experimental requirements, and the locations of the sampling points are shown in Figure 1.

After the dust sample was collected, it was initially crushed with a small hammer. The larger block sample was then crushed to a size of 12 mm in size. The precrushed dust sample was then put into the XPS-250 × 150 roller crusher for a second round of crushing. The resulting crushed dust sample was then sieved with a 100 mesh sieve to remove any uncrushed particles. Following this, the final dust samples could be obtained. After sampling, a series of experiments were conducted to analyze the dust samples, including the measurement of the aqueous solution's pH value, the contact angle of the dust, and the saturated moisture content, as shown in Table 1.

**Table 1. Physical Properties of Dust**

| Test items | pH | Contact angle (deg) | Saturation humidity ratio (%) |
|---|---|---|---|
| Results | 6.1 | 13.4 | 22 |

**2.2. Reagents Required for the Experiment.** The purity and source of the reagents required for the preparation of the composite DSP are listed in Table 2.

**2.3. Preparation of the DSP Formula.** Guar gum, as the main body of the DSP, has many advantages, such as excellent adhesion, a wide range of sources, nontoxicity, and harmlessness. However, there are still shortcomings such as insufficient resistance to high temperatures and easy decomposition by microorganisms, etc. In order to enhance the evaporation resistance of the DSP and the lasting performance of the dust, it is necessary to close the active hydroxyl group in the molecular structure of the guar gum; as such, in this research, the GG was carried out with this modification.

**Table 2. Reagents Required for Preparing Composite DSP**

| Reagent | Purity | Source |
|---|---|---|
| Guar gum (GG) | ≥99 | Shanghai Boer Chemical Reagent Co., Ltd. |
| Active group modifier (TCS) | ≥97 | Shanghai Aladdin Biochemical Technology Co., Ltd. |
| $NaHCO_3$ | ≥99.9 | Shanghai Boer Chemical Reagent Co., Ltd. |
| Anhydrous ethanol | ≥99.5 | Shanghai Boer Chemical Reagent Co., Ltd. |
| Polyethylene glycol (PEG) | ≥99 | Beijing Innokai Technology Co., Ltd. |
| Rhamnolipids (CAS) | ≥97 | Shanghai Boer Chemical Reagent Co., Ltd. |

*2.3.1. Modification of GG.* The appropriate amount of GG solution was stirred until it was completely dissolved and then placed in a three-necked flask. At a specific temperature level, the monochloro homotriazine-type reactive group modifier (TCS) was slowly added to modify the GG. After sufficient stirring, the sodium bicarbonate solution was gradually added to the flask. The product was washed three times with anhydrous ethanol after the reaction had continued for a certain period of time. The extracted solution was cooled to room temperature, and the product underwent a drying process at 60 °C until it achieved a stable quality, resulting in the formation of GGTCS. Subsequently, the obtained product was finely powdered and stored in a flask. The chemical process of GG modification is shown in eq 1.

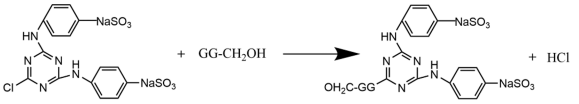


(1)

*2.3.2. Synthesis of Composite DSP.* A beaker was prepared by adding 100 mL of deionized water, which was subsequently placed on the DF-S101 magnetic stirrer. The temperature was maintained at a constant 45 °C, and the magnetic stirring was set to three gears. Then, 0.2 mL of polyethylene glycol was slowly added to achieve uniform dispersion. Then, 0.4 g of rhamnose lipids was slowly added and stirred for 5 min to ensure its uniform dissolution in the solution. The above solution was transferred to an ultrasonic disperser. Then, 0.6 g of modified guar gum powder was added to the HN-12N ultrasonic disperser. The ultrasonic dispersion was carried out for 10 min to obtain the homogeneous composite DSP solution. The preparation process is shown in Figure 2.

**2.4. Fourier Transform Infrared Spectroscopy (FTIR).** The Nicolet iS-10 model was manufactured by Thermo fisher



https://doi.org/10.1021/acsomega.3c07734
ACS Omega 2024, 9, 3746−3757

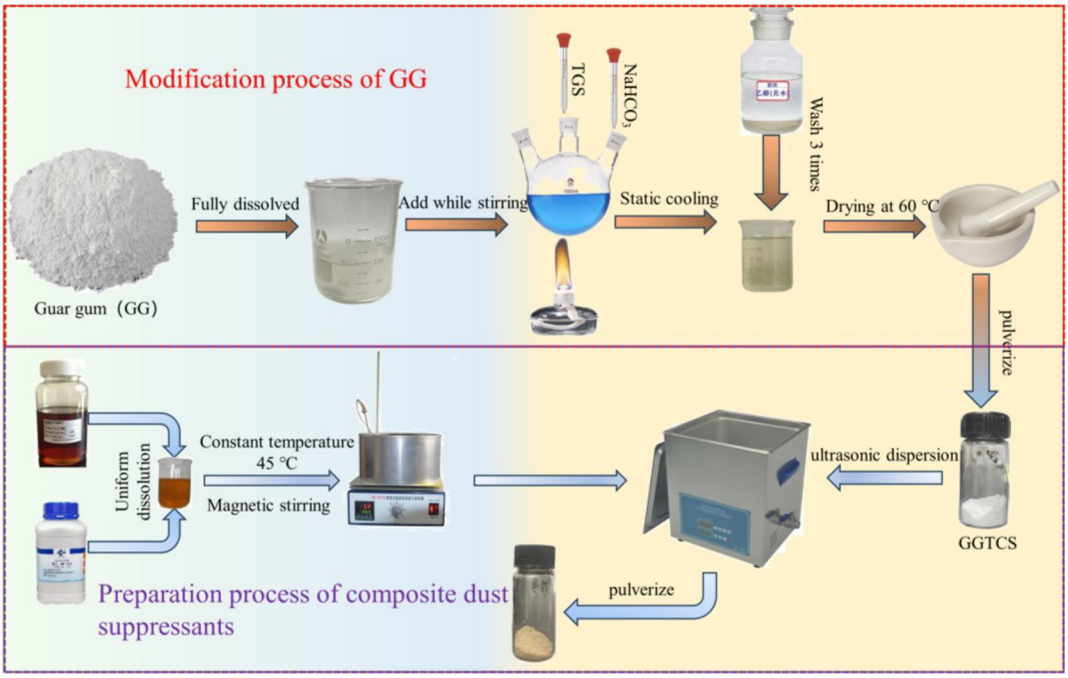


**Figure 2.** Flowchart for preparation of the composite DSP.

Co., Ltd. in situ Fourier transform infrared (FTIR) method was used to test the DSP powder to obtain the change results in the functional groups between the GGTCS composite DSP and the GG composite DSP, as well as to analyze whether the modification was successful or not. In this experiment, the samples for IR spectroscopic testing were prepared by a potassium bromide compression method. The prepared dust samples were sieved through a 100-mesh sieve, and appropriate amounts of sieved guar gum composite DSP powder and modified guar gum DSP powder were taken separately and mixed with dry KBr in a ratio of 1:80. Then, the mixture was put into an agate mortar and ground for a further 10 min and then placed into a tablet press. The samples were continuously pressed at a pressure of 2 MPa for 5 min to form a sample tablet with a thickness between 0.3 and 0.5 mm. The scanning band was set to 400−4000 $cm^{-1}$, the resolution was set to 4 $cm^{-1}$, and the number of scans was set to 32 times.

**2.5. Contact Angle Measurement of DSP Solutions.** The dynamic contact angle was measured using a Dataphysics OCA40 contact angle measuring instrument (manufactured by dataphysics Co., Ltd.) and powder compaction molds. The images returned by the Dataphysics OCA40 were used to analyze the effects of the different components of DSP and water on the contact angle of the dust and then to illustrate the difference in the wetting effects of different components of DSPs and the water on the dust.

First, the dust sample was compressed by pouring 0.9 g of it into the pressing mold of the 769YP-24B powder tablet press and pressurizing it at 10−20 MPa to produce a cake-like sample. Next, the sample was placed on the carrier table of the contact angle tester and analyzed by using One Attension software. The angle of contact between the droplet and the sample surface was determined by rotating the dropper knob until the liquid was released. The experiment was repeated three times to measure the contact angle of the solution and dust specimen surface.

**2.6. Preparation of Experimental Samples Combined with Dust.** The dust sample prepared with a 100 mesh sieve in Section 2.1 of this paper was measured with an analytical balance, resulting in 40 g. The sample was divided into four equal portions and spread out in Petri dishes. In the first Petri dish, 10 mL of tap water was evenly and slowly sprayed, and it was recorded as Sample 1. In the second Petri dish, a mixture of 9 mL of tap water and 1 mL of a modified guar gum composite DSP was evenly and slowly sprayed, and it was recorded as Sample 2. Similarly, in the third Petri dish, a mixture of 9 mL of tap water and 1 mL of a modified guar gum composite DSP was sprayed evenly and slowly, and it was recorded as Sample 3. Finally, in the fourth Petri dish, a modified guar gum composite DSP was evenly and slowly sprayed without dilution, and it was recorded as Sample 3.

**2.7. Scanning Electron Microscopy (SEM).** In order to analyze the microscopic morphology of the samples and to study and analyze their wind erosion resistance and DSP bonding properties, scanning electron microscopy experiments (SEM) were used to characterize the samples for the experiments. A ZEISS EVO 18 analytical scanning electron microscope (manufactured by zeiss Co., Ltd.) was used to take pictures, which has a magnification of 5−1 million times and an accelerating voltage parameter of 0.2−30 kV.

The four experimental sample powders were uniformly ground into solid powder particles, and the conductive adhesive was tightly bonded to the metal strips; meanwhile, about 0.1 mg of the sample powder was scooped up with a medicine spoon and evenly spread on the conductive adhesive. These were then gold sprayed with a HITACHI Mciooo type gold sprayer, the current size was set to less than 10 mA, the vacuum degree was set to 4 mmHg, and the time was set to 300 s. They were then photographed for their microscopic morphology.

**2.8. Thermogravimetric Experiment (TG).** In order to study the thermal stability of the GGTCS composite DSP, thermogravimetric experiments were conducted for Samples 1


https://doi.org/10.1021/acsomega.3c07734
ACS Omega 2024, 9, 3746−3757

and 2 and sprayed with DSP. However, Sample 3 was sprayed with water. The experiments were carried out using an STA 7200 Thermogravimetric Analyzer manufactured by Nippon Co., Ltd.

Before the experiment, the thermogravimetric analyzer was connected to the gas cylinder, and then the instrument was turned on to warm up. A crucible was taken out and filled with about 10 mg of the experimental sample, followed by placing it in the thermogravimetric analyzer. In the heating program, the heating rate was set to 10 °C/min, the heating interval was from 20 to 700 °C, the air flow rate was 100 mL/min, and then the program was opened to raise the temperature for thermogravimetric analysis. When the trend of the TG curve and DTG curve is used, the temperature of the four main characteristic points during the heating process of the sample can be analyzed.

**2.9. Wind Erosion Resistance Test (WER).** In order to quantitatively analyze the improvement of the wind erosion resistance of the dust by the GGTCS composite DSP, a WER test was conducted by using a wind turbine to simulate the field conditions. Four sets of 100 g of dust samples were weighed and placed uniformly on a circular Petri dish with a diameter of 252 mm and a height of 18 mm. The prepared GG composite DSP and GGTCS composite DSP were uniformly sprayed onto the dust samples. A volume of 3 mL of DSP was sprayed at one time in order to prevent any nonuniformity in spraying that could occur if the spraying needs to be repeated several times. At the same time, a group of samples were sprayed with tap water as a control group. After spraying and drying at room temperature, the samples were subjected to a consistent temperature of 60 °C in an oven for a duration of 5 h. Following complete evaporation of the water within the samples, they were subsequently resprayed with the composite DSP. This spraying process was reiterated three times. In order to simulate the field environment, the dried dust samples were crushed, a CL-3003 cantilever beam impact tester was used to crush the four groups of Petri dishes with the same force, and a wind erosion test was conducted after the dust samples were loosened.

The wind erosion was tested by using a fan to test the three groups of samples at different angles and different wind speeds. The samples were raised to 15°, 30°, and 45° from the plane using a stand, and then the fan was turned on to set the wind speeds to 6 and 10 m/s for the tests. This was carried out for 3 min for each group of experiments. The mass residual value of the samples during the test was used as a measure of wind erosion resistance.

**2.10. Environmental Hazard Testing.** *2.10.1. pH of the Composite DSP.* In this study, in order to investigate the change in acidity and alkalinity of the DSP combined with dust, 10 mL of GGTCS composite DSP and 30 g of dust samples were placed in a beaker, and the pH change was monitored using a pH 100 hand-held pH meter. The readings were recorded every 10 min during the first hour and then every hour hence between 1 and 6 h.

*2.10.2. Corrosion Test of Composite DSP.* In the spraying process, the composite DSP may cause corrosion after contact with spraying vehicles, facilities, tools, transportation pipelines, etc. In this research, we conducted a uniform corrosion performance total immersion test based on the "Uniform Corrosion Test Method in the Laboratory". The primary materials under investigation, including mild steel, stainless steel, and aluminum alloy, were selected to assess their corrosion behavior when in contact with the composite DSP. Each sample had dimensions of 25 mm ($W$) × 50 mm ($L$) × 5 mm ($H$), and the test duration was set at 72 h. At the conclusion of the test, the corrosion rate was determined using eq 2.

$$R = \frac{8.76(M - M_1) \times 10^7}{DTS} \quad (2)$$

where $R$ is the corrosion rate, mm/a; $M$ is the mass of the sample before testing, g; $M_1$ is the mass of the sample after the test, g; $D$ is the material density, kg/m$^2$; $T$ is the testing time, h; and $S$ is the total area of the sample, mm$^2$.

## 3. RESULTS AND DISCUSSION

**3.1. FTIR Results.** Figure 3 shows the IR spectral profiles of the GG and GGTCS DSPs before and after chemical

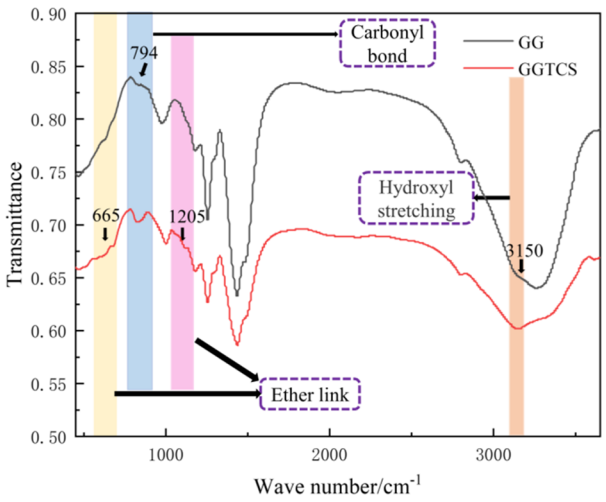


**Figure 3.** FTIR spectra of the different samples.

modification. Figure 3 illustrates the comparison between the curves of GG and GGTCS. It is apparent from the figure that the IR spectra of GG remain unchanged even after undergoing chemical modification, which shows that the basic properties of guar gum were not obviously changed. In the IR spectra of the GG, there are characteristic absorption peaks at 794 cm$^{-1}$ corresponding to the C−Cl bond, and at 3150 cm$^{-1}$ for the hydroxyl group, this is highly consistent with the conclusions drawn by other researchers.[33,34] However, the characteristic absorption peak of the C−Cl bond at 794 cm$^{-1}$ in the IR spectrogram of the GG disappeared in the GGTCS. This result is in line with the expected effect of the experiment and mutually confirms with the experimental results of other researchers and indicates that the TCS has reacted with the GG in the presence of sodium bicarbonate, and that the TCS has been successfully introduced into the GG to produce the desired product, GGTCS.[35] The generation of the ether bond stretching vibration and bending vibration peaks at 665 and 1205 cm$^{-1}$ also indicates the success of the modification and the formation of the ether bond by the reaction between the GG and TCS. In addition, the disappearance of the characteristic absorption peak of the hydroxyl group at 3150 cm$^{-1}$ also indicated the primary amine reaction between a chlorine atom and the hydroxyl group on the GG. In the reaction, the chloride ion ($Cl^-$) attacks the hydroxyl group with a higher electron density to form the imine intermediate


https://doi.org/10.1021/acsomega.3c07734
ACS Omega 2024, 9, 3746−3757

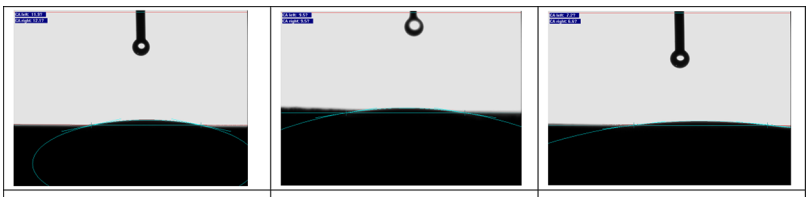

(a) Contact angle between the water and dust sample. (b) Contact angle between the GG and dust sample. (c) Contact angle between the GGTCS and dust sample.

**Figure 4.** Experimental results of the contact angle.

(ROCl). The imine then undergoes an elimination reaction, losing one molecule of hydrochloric acid (HCl) to produce the modified GGTCS.

**3.2. Contact Angle Experiment Results.** The contact angle between water and the DSP on the dust surface is assessed using a contact angle tester. This is for a visual comparison of the wetting properties of water and DSP on the dust sample. During the experiment, the contact angle with the dust is recorded by a high-speed camera, and the detailed results are presented in Figure 4. In this figure, the black plane represents the dust sample; the curved protruding portion represents water or dust suppressant, and the left and right angles of the two parts represent the left and right contact angles.

From Figure 5, it can be seen that the L and R contact angles of water are 12.6° and 12.3°, respectively. The L and R contact

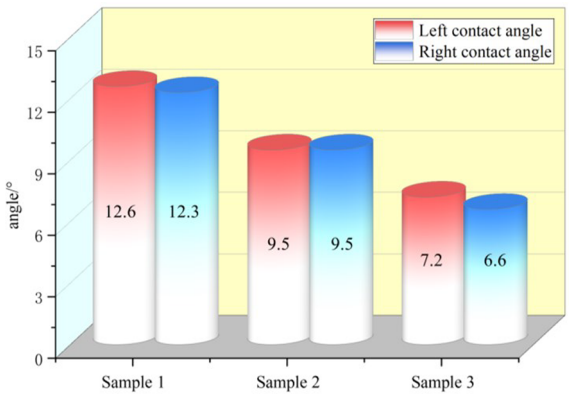


**Figure 5.** Comparison of the influence of different solutions on the contact angle of dust samples.

angles of the GG composite DSP were 9.5,°, and the L and R contact angles of the GGTCS composite DSP for dust were 7.2 and 6.6. The smaller the contact angle for the dust samples, the better the wetting performance of the DSP. In Figure 5, the contact angles of the water and DSP for the dust samples can be clearly compared, and the contact angle of the DSP is obviously smaller than that of water, which indicates that the DSP had a better wettability for dust. The contact angle of the GGTCS composite DSP is also smaller than that of the GG composite DSP, which indicates that the modification of the TCS is successful and that the modification makes the hydrophilicity inside the guar molecules increase; as such, the contact angle is also reduced.

**3.3. SEM Characterization.** The dust samples are processed in different ways, and the microstructure of Samples 1−4 is observed and analyzed by SEM Figure 6 shows the sample particles magnified 2000x via SEM Figure 6a shows that most of the dust particles in Sample 1 are small and loosely distributed in the visible range. The gap between the adjacent particles is spacious, and the surface appears relatively glossy. Figure 6b shows that, compared with that of Sample 1, the gap between the adjacent dust particles in Sample 2 is greatly reduced. In addition, it shows that there are numerous fine particles adhering to the surface of the dust, and it can be clearly seen that some of the small particles of the dust aggregated together to form larger particles. Composite DSPs can adhere to dust particle surfaces or occupy dust particle pores, thereby reducing the porosity of dust and producing a certain degree of wind erosion resistance. Figure 6 shows the morphology of the modified dust, and compared with Sample 2, it can be clearly seen that the particles formed by agglomeration are larger and more compact, which can be observed through the morphology. This is due to the modified guar gum bonding performance being better, and that it can achieve the same effect of agglomeration while using less composite DSP. Figure 6d shows the morphology of the sample treated with a higher concentration of the composite DSP. Figure 6d shows that the degree of the agglomeration of dust particles is further increased but also that the effect of the increase is not obvious enough, which indicates that a single increase in the concentration of a binder does not greatly improve the effect of the agglomeration of dust.

Figure 7 represents the sample particles magnified 200x with SEM. As shown in Figure 7a, most of the dust in Sample 1 existed in the form of small particles. In addition, a small portion of the dust particles forms lumps, which is due to the fact that the dust still has a small amount of moisture inside and that the lumps are formed after drying. Figure 7 shows that almost all of the dust was agglomerated into lumps after adding unmodified guar gum DSP, and the degree of agglomeration was obviously better than that of Sample 1, but the fine granular dust is still scattered around the lumps. While Figure 7c shows that the size of agglomeration of the modified DSP for dust agglomeration is basically unchanged, the fine particles around the large pieces of dust evidently disappeared; this is because the adsorption of the modified guar gum for the fine particles is much stronger than that before the modification. This undoubtedly further improves the wind erosion resistance of the dust. Figure 7d shows the dust of Sample 4 after increasing the concentration of DSP spraying. The SEM image in Figure 7d shows that the massive dust increases slightly compared with Figure 7c, and that the number of the agglomerates increases.

**3.4. TG Test Results.** The thermogravimetric curves in Figures 8, 9, and 10 correspond to the TG-DTG outcomes for samples 1, 2 and 3, respectively. Examining the TG curves, it becomes evident that the pyrolysis process of these samples encompasses three stages: initial water loss and drying,



https://doi.org/10.1021/acsomega.3c07734
ACS Omega 2024, 9, 3746−3757

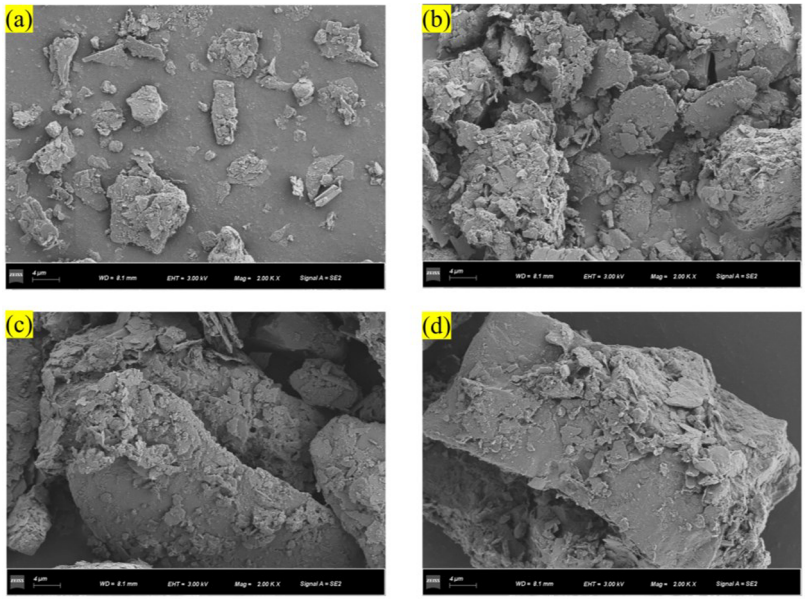


**Figure 6.** (a–d) 2000× SEM micrographs of samples after different treatments.

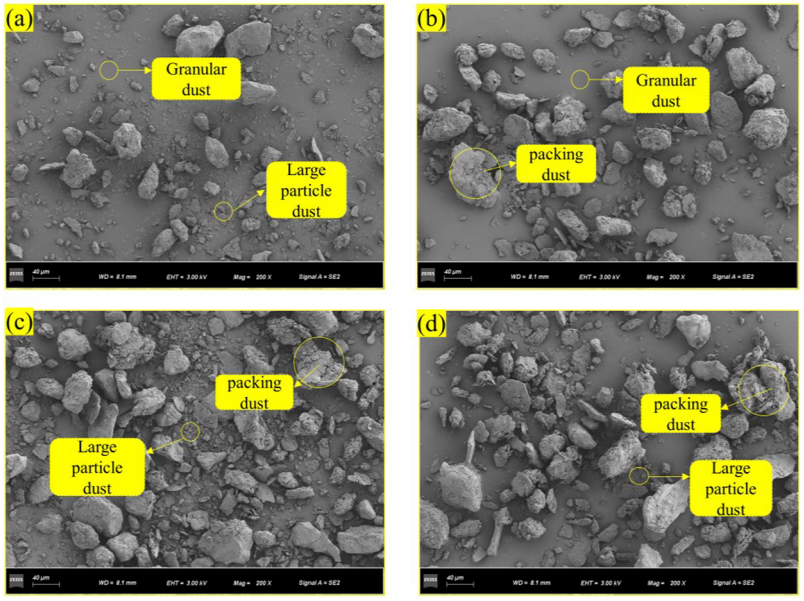


**Figure 7.** (a–d) The 200× SEM micrographs of samples after different treatments.

followed by a phase of rapid thermal decomposition, culminating in a stage of gradual decomposition. When the temperature reaches temperature T1 in Table 4, this indicates that the sample reaches the first extreme point of thermal decomposition rate at this point, which indicates that the rate of the low melting point volatiles in the sample molecules reach the maximum and that a slight mass loss occurrs between T1 and T2. After that, it reaches about 100 °C and enters the water loss drying phase. The T2 temperature point is the temperature point where the rate of free water evaporation and detachment reaches a maximum and where the sample then enters the mass stabilization phase. In the 250−300 °C temperature range, the TG curve exhibits a rapid decline, constituting approximately 18% of the overall mass loss. Point T3 represents the peak rate of the mass loss within this interval, which is primarily attributed to the exothermic reactions resulting from chemical bond breakage. As the temperature increases, more chemical bonds break and the molecular chains of the polymer also undergo reactions within this temperature range. This results in the destruction of the stabilized structure and the volatilization of more components, thus, leading to a reduction in mass. Between 450 and 500 °C, slight mass loss occurs continuously due to the decomposition of the residual material. The temperature point at which the rate of loss reached a maximum is T4. Moreover, 250−300 °C and 450−500 °C are called the rapid thermal decomposition stages, and the slow decrease in sample mass in the stage after 500 °C is called the slow decomposition stage.

Through a horizontal comparison, shown in Table 3, the weight loss rates of Sample 3 at T1 and T2 (0.067%/min and 0.24%/min, respectively) were significantly lower than those of Sample 2 (0.071%/min and 0.30%/min, respectively) and



https://doi.org/10.1021/acsomega.3c07734
ACS Omega 2024, 9, 3746−3757

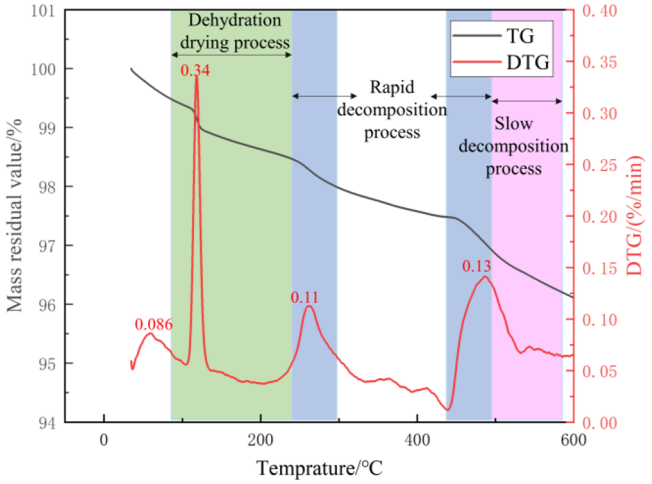


**Figure 8.** Thermogravimetric curve of Sample 1.

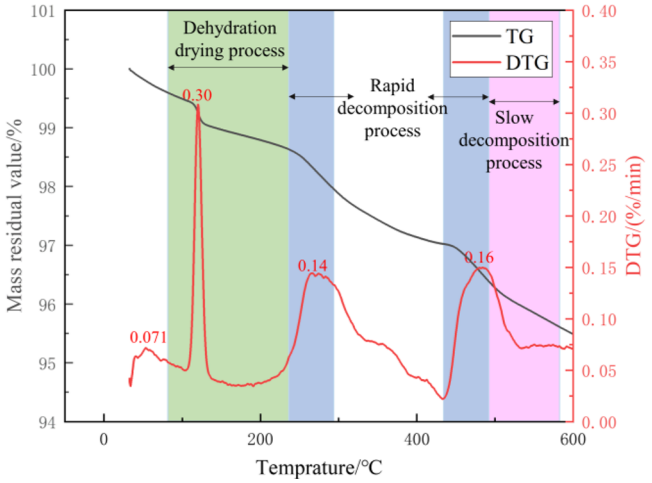


**Figure 9.** Thermogravimetric curve of Sample 2.

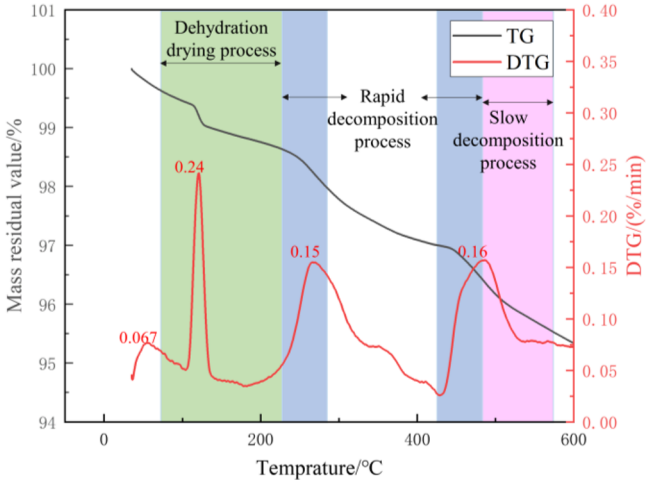


**Figure 10.** Thermogravimetric curve of Sample 3.

Sample 1 (0.086%/min and 0.34%/min, respectively) by approximately 6.0% and 28%, respectively. This difference indicates that the DSP has a significant inhibitory effect on the evaporation of internal moisture and low melting point substances when the temperature is lower than T2, and the comparison of Samples 2 and 3 can also indicate that the

**Table 3. Composition Table of the Experimental Samples**

| Sample | Main materials | Water (mL) | Dust sample (g) |
|---|---|---|---|
| 1 | - | 10 | 10 |
| 2 | 1.0 g GG Composite DSP | 9 | 10 |
| 3 | 1.0 g GGTCS Composite DSP | 9 | 10 |
| 4 | 2.0 g GGTCS Composite DSP | 8 | 10 |

**Table 4. Sample Thermogravimetric Characteristic Temperature Point**

| | Characteristic temperature value (°C) (mass loss rate/(%/min)) | | |
|---|---|---|---|
| Sample | 1 | 2 | 3 |
| T1 | 58.49 (0.086) | 54.07 (0.071) | 54.17 (0.067) |
| T2 | 118.01 (0.34) | 120.17 (0.30) | 121.06 (0.24) |
| T3 | 263.33 (0.11) | 275.17 (0.14) | 265.60 (0.15) |
| T4 | 485.86 (0.13) | 479.68 (0.16) | 486.21 (0.16) |

modified guar gum's evaporation resistance has been significantly optimized. This is especially the case when the T1 (50−60 °C) temperature point is reached, as this temperature range is very close to the temperature of the Guangzhou surface when it is exposed to sunlight for a long time. In this case, the GGTCS composite DSP shows excellent evaporation resistance, which is a property of great practical importance in real applications. When the temperature reaches T3 and T4, the weight loss rates of Sample 1 (0.11%/min and 0.13%/min) were significantly lower than those of Samples 2 (0.14%/min and 0.16%/min, respectively) and 3 (0.15%/min and 0.16%/min, respectively). This is due to the fact that with the increase in the temperature, the organic compound in the DSP starts to decompose and evaporate. However, Sample 1 does not add any DSP; as such, the weight loss rate of Sample 1 is the lowest during the rapid thermal decomposition stage. This indicated that the composite DSP is still decomposable at high temperatures and that there is no problem of permanent residue.

**3.5. Results of the Wind Erosion Resistance Test.** To provide a more realistic simulation and to restore the scene situation, the experiment is divided into three steps. Figure 11 is the step diagram of the WER. Among them, Figure 1-(a) shows the samples sprayed with different dust suppression compositions. Figure 11-(b) shows the dust samples after wind erosion and drying at a high temperature. Figure 11-(c) shows the dust samples after pressure crushing, and Figure 11-(d) shows the dust samples after high temperature drying of the samples after wind erosion, where the order of Samples 1−4 shown in Figure 11-(a) is labeled.

The respective residual masses of the dust under wind erosion are obtained for Samples 1−4 after 3 min of experiments are conducted for each sample at different wind speeds and angles. The detailed data are shown in Table 5.

Table 5 shows that when the wind speed is lesser than 6 m/s, both water and DSP can ensure the dust fixation rate above 60%. In the comparison of the DSP with different components or concentrations, it is found that the difference between the residual values of Sample 2 and Sample 3 under the conditions of inclination angles of 15° and 30° is large and reached 9.6% and 9.7%, respectively. The difference between the residual values under an inclination angle of 45° is only 2.4%. This indicates that under the conditions of a small inclination angle, only the fine dust is blown away. The large particles of dust are


https://doi.org/10.1021/acsomega.3c07734
ACS Omega 2024, 9, 3746−3757

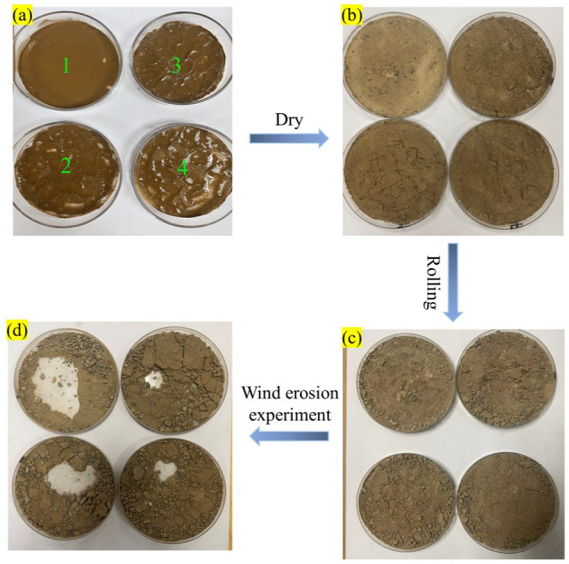


**Figure 11.** (a–d) Procedure diagram for the wind erosion resistance test.

**Table 5. Residual Mass of Dust under Different Wind Speeds and Dip Angles**

| | Residual mass (g) | | | | | |
|---|---|---|---|---|---|---|
| | Wind speed 6 m/s | | | Wind speed 10 m/s | | |
| Dip angle | 15° | 30° | 45° | 15° | 30° | 45° |
| Sample 1 | 67.3 | 48.5 | 30.4 | 63.8 | 36.2 | 22.3 |
| Sample 2 | 80.2 | 62.7 | 50.9 | 77.3 | 55.1 | 49.8 |
| Sample 3 | 89.8 | 72.4 | 53.3 | 83.6 | 70.8 | 54.6 |
| Sample 4 | 90.2 | 74.6 | 52.0 | 86.6 | 70.3 | 58.4 |

unlikely to be blown away due to their large mass and the role of internal water, which also indicate that the modified guar gum has a particularly significant bonding effect on the small particles.

When the wind speed increased to 10 m/s, the dust fixation rate of the aqueous solution decreased rapidly, with an average decrease of 7.97% for each inclination angle. This is because the bonding force of the water is weak after drying, and it is difficult to fix both powdery and granular dust at this time. When the wind speed increases, the medium-sized dust is blown away and part of the large-sized dust is eroded, thereby resulting in a reduction in the total mass. The residual values of the samples after spraying the DSP are greatly improved compared with those of the samples sprayed with water. In addition, even if the wind speed increased from 6 to 10 m/s, the fixation rate of the dust samples at each inclination only decreased by 3.03% and 3.87% on average after spraying the GGTCS composite DSP and GG composite DSP. This is found to be much lower than that of the sprayed aqueous solution by 7.97%. It also indicated that the DSP has a bonding and curing effect on both large and small particles in the dust. A longitudinal comparison showed that the inclination angle had a significant impact on the residual value of dust quality. When other conditions are the same, the inclination angle can be reduced from 45° to 15° and the maximum residual value of the dust quality can be increased to 2.63 times. In the most favorable condition for dust fixation(6 m/s, 15°), Sample 4 exhibits a dust fixation rate 1.3 times that of Sample 1. However, under the most unfavorable conditions for dust fixation(10 m/s, 45°), Sample 4's dust fixation rate is 2.6 times that of Sample 1. This result demonstrates the excellent resistance of the GGTCS composite DSP in adverse environmental conditions.

It can be seen that the DSP developed in this research has good wind erosion resistance and that the sprayed DSP solution can form a solidified layer on the surface of dust samples through curing, absorption, bonding, and film-forming, which can effectively reduce the dust pollution caused by wind erosion. Compared with the control group, the sprayed DSP effectively improved the wind erosion resistance of the dust samples, which can resist wind erosion in the natural environment and prolong the action time of the DSP.

### 3.6. Results of Environmental Hazard Testing.

*3.6.1. pH Value of the Solution.* The pH value of GGTCS composite DSP has a significant environmental impact after spraying. High pH value will lead to land salinization, and low pH value will increase the corrosiveness of the transport pipeline. Figure 12 shows the change of pH value in different

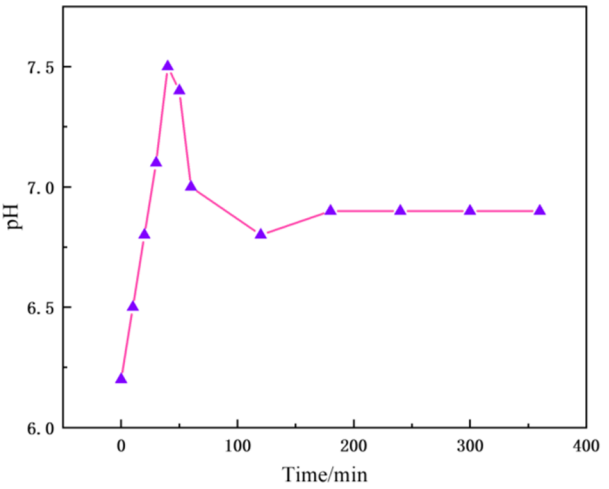


**Figure 12.** Changes in pH of the suppressant at different time.

time, the pH value of the solution increased from 6.2 to 7.5 in 40 min, and after 40 min, the pH value gradually decreases, and finally stabilized at about 6.9. This means that the reacted GGTCS composite DSP is almost neutral, and has almost no effect on the ecological environment.

*3.6.2. Results of the Corrosion Test.* The uniform corrosion results of the composite DSP are listed in Table 6. Whether for

**Table 6. Test Results with Uniform Corrosivity**

| | Uniform corrosion rate/(mm/a) | | |
|---|---|---|---|
| Sample | Mild steel | Inoxidable steel | Al Alloy |
| Sample 1 | 0.065 | 0.034 | 0.058 |
| Sample 3 | 0.065 | 0.031 | 0.052 |
| Sample 4 | 0.073 | 0.030 | 0.049 |

a high concentration or low concentration of DSP, for inoxidable steel and Al alloys, the uniform corrosion rate of the DSP is slightly lower than that of tap water. And for mild steel, a high concentration of the DSP gives a uniform corrosion rate of 0.073, slightly higher than that of tap water at 0.065. The comprehensive result for the DSP's corrosive strength is basically the same as that for tap water. It can be


https://doi.org/10.1021/acsomega.3c07734
ACS Omega 2024, 9, 3746−3757

seen that the dust suppressant formulated in this experiment has a weak corrosivity and can be used for dust suppression in building construction. Stainless steel materials can be used to prevent the corrosion of pipelines.

## 4. CONCLUSIONS

In this study, a dust suppressor with a compound effect of dust suppression and environmental disturbance resistance was prepared using GG, CAS, and PEG as raw materials. The chemical modification enhanced GG's hydrophilicity, reduced its reactivity, and improved its thermal stability. This approach fully exploited GG's potential as a DSP. The main conclusions are as follows:

(1) According to the results of FTIR experiments, the disappearance of C−Cl bond absorption peaks at 794 $cm^{-1}$, the generation of ether bond stretching and bending vibration peaks at 665 and 1205 $cm^{-1}$, and the disappearance of hydroxyl group characteristic absorption peaks at 3150 $cm^{-1}$ all indicate that the modification of GG was successful. GG reacted with the modifier to produce GGTCS under the conditions described in this paper, and the active hydroxyl group in GG was replaced.

(2) According to the results of the TG experiments, the weight loss rates of the dust samples treated with the GGTCS composite DSP at T1 and T2 (0.067%/min and 0.24%/min, respectively) were significantly lower than those of Sample 2 with the GG composite DSP (0.071%/min and 0.30%/min, respectively) and Sample 1 with tap water (0.086%/min and 0.34%/min, respectively), by 6.0% and 28%, respectively. This difference indicated that the modified guar gum DSP had a significant inhibition effect on the volatilization of water and low melting point substances inside the dust at temperatures lower than T1, and that it had a good thermal stability.

(3) The results of the SEM experiments show that the GGTCS composite DSP can form more compact particles when acting on dust, and that the GGTCS composite DSP can stick on the surface of dust particles or infiltrate their pores, thus effectively reducing the porosity of the dust material. This reduction in porosity contributes to a certain level of wind erosion resistance. And, through the experiment, it shows that a single increase in the concentration of the binder does not improve the effect of dust agglomeration.

(4) After spraying GGTCS composite DSP and GG composite DSP in the wind erosion resistance test, even if the wind speed increases from 6 to 10 m/s, the solidification rate of the dust samples at each inclination angle only decreased by 3.03% and 3.87% on average, which is much lower than that of 7.97% in the case of spraying aqueous solution. This indicates that the DSP has a bonding and solidification effect on the large and small particles in the dust.

(5) The pH value of the GGTCS composite DSP was basically maintained at 6.9, and the corrosion strength was basically the same as that of tap water. It can be seen that the dust suppressant formulated in this experiment has weak corrosivity and could be used for dust suppression in building construction. Stainless steel materials can be used to prevent the corrosion of pipelines.

(6) This study has demonstrated the excellent performance of GGTCS DSP in resisting harsh environmental conditions and its sustained dust suppression capabilities. Subsequent research can focus on innovative methods for calculating experimental data and conducting on-site experiments to analyze dust suppression effectiveness.

## AUTHOR INFORMATION


### Corresponding Authors

**Shijie Peng** − *State Key Laboratory of High-Efficient Mining and Safety of Metal Mines (University of Science and Technology Beijing), Ministry of Education, Beijing 100083, PR China;* orcid.org/0009-0001-4418-0045; Email: 350976764@qq.com

**Hongsheng Wang** − *Inst Risk Assessment and Control, Guangdong Technol Ctr Work Safety Co., Ltd., Guangzhou 510050, PR China; State Key Laboratory of High-Efficient Mining and Safety of Metal Mines (University of Science and Technology Beijing), Ministry of Education, Beijing 100083, PR China;* Email: 757161231@qq.com

**Yinghua Zhang** − *State Key Laboratory of High-Efficient Mining and Safety of Metal Mines (University of Science and Technology Beijing), Ministry of Education, Beijing 100083, PR China;* orcid.org/0000-0003-1129-6938; Email: zhangyinghuaustb@sina.com

### Authors

**Hao Ding** − *Inst Risk Assessment and Control, Guangdong Technol Ctr Work Safety Co., Ltd., Guangzhou 510050, PR China; State Key Laboratory of High-Efficient Mining and Safety of Metal Mines (University of Science and Technology Beijing), Ministry of Education, Beijing 100083, PR China*

**Zhian Huang** − *State Key Laboratory of High-Efficient Mining and Safety of Metal Mines (University of Science and Technology Beijing), Ministry of Education, Beijing 100083, PR China*

**Jinyang Li** − *State Key Laboratory of High-Efficient Mining and Safety of Metal Mines (University of Science and Technology Beijing), Ministry of Education, Beijing 100083, PR China*

**Ruixiang Wang** − *State Key Laboratory of High-Efficient Mining and Safety of Metal Mines (University of Science and Technology Beijing), Ministry of Education, Beijing 100083, PR China*

**Pengfei Wang** − *Work Safety Key Lab on Prevention and Control of Gas and Roof Disasters for Southern Coal Mines, Hunan University of Science & Technology, Xiangtan 411201, PR China*

Complete contact information is available at: https://pubs.acs.org/10.1021/acsomega.3c07734


### Notes

The authors declare no competing financial interest.

## ACKNOWLEDGMENTS

The authors acknowledge the financial support of project Nos. 51974015 and 51474017 provided by the National Natural Science Foundation of China; project No. SMDPC202101 provided by the Key Laboratory of Mining Disaster Prevention



https://doi.org/10.1021/acsomega.3c07734
ACS Omega 2024, 9, 3746−3757

and Control (Shandong University of Science and Technology); project Nos. FRF-IC-20-01 and FRF-IC-19-013 provided by the Fundamental Research Funds for the Central Universities; project No. 2018YFC0810601 provided by the National Key Research and Development Program of China; project No. 2020CXNL10 provided by the Fundamental Research Funds for the Central Universities (China University of Mining and Technology); project No. WS2018B03 provided by the State Key Laboratory Cultivation Base for Gas Geology and Gas Control (Henan Polytechnic University); and project No. E21724 provided by the Work Safety Key Lab on Prevention and Control of Gas and Roof Disasters for Southern Coal Mines of China (Hunan University of Science and Technology).

## REFERENCES

(1) Hong, J.; Kang, H.; Jung, S.; Sung, S.; Hong, T.; Park, H. S.; Lee, D.-E. An empirical analysis of environmental pollutants on building construction sites for determining the real-time monitoring indices. *Build Environ.* **2020**, *170*, 106636.
(2) Joshi, K.; Navalgund, L.; Shet, V. B. Water pollution from construction industry: An introduction. *Int. J. Environ. Res. Public Health.* **2022**, *12*, 245−257.
(3) Srivastav, A. L.; Dhyani, R.; Ranjan, M.; Madhav, S.; Sillanpää, M. Climate-resilient strategies for sustainable management of water resources and agriculture. *Environ. Sci. Pollut Res. Int.* **2021**, *28* (31), 41576−41595.
(4) Lillini, R.; Tittarelli, A.; Bertoldi, M.; Ritchie, D.; Katalinic, A.; Pritzkuleit, R.; Launoy, G.; Launay, L.; Guillaume, E.; Žagar, T.; Modonesi, C.; Meneghini, E.; Amati, C.; Di, Salvo. F.; Contiero, P.; Borgini, A.; Baili, P. Water and Soil Pollution: Ecological Environmental Study Methodologies Useful for Public Health Projects. A Literature Review. *Rev. Environ. Contam Toxicol.* **2021**, *256*, 179−214.
(5) Andersson, M.; Ottesen, R. T.; Volden, T. Building materials as a source of PCB pollution in Bergen, Norway. *Sci. Total Environ.* **2004**, *325* (3), 139−144.
(6) Obmiński, A. Asbestos cement products and their impact on soil contamination in relation to various sources of anthropogenic and natural asbestos pollution. *Sci. Total Environ.* **2022**, *848*, 157275.
(7) Song, H. Y.; Li, J. X.; Li, L. J.; Dong, J.; Hou, W. X.; Yang, R.; Zhang, S. W.; Zu, S. D.; Ma, P. F.; Zhao, W. J. Heavy Metal Pollution Characteristics and Source Analysis in the Dust Fall on Buildings of Different Heights. *Int. J. Environ. Res. Public Health.* **2022**, *19* (18), 11376.
(8) Corvo, F.; Reyes, J.; Valdes, C.; Villasenor, F.; Cuesta, O.; Aguilar, D.; Quintana, P. Influence of air pollution and humidity on limestone materials degradation in historical buildings located in cities under tropical coastal climates. *Water Air Soil Pollut.* **2010**, *205*, 359−375.
(9) Tjoe, Nij. Evelyn.; Hilhorst, Simone.; Spee, Ton.; Spierings, Judith.; Steffens, Friso.; Lumens, Mieke.; Heederik, Dick. Dust control measures in the construction industry. *Ann. Occup. Hyg.* **2003**, *47* (3), 211−218.
(10) Tong, R.; Cheng, M.; Zhang, L.; Liu, M.; Yang, X.; Li, X.; Yin, W. The construction dust-induced occupational health risk using Monte-Carlo simulation. *J. Clean Prod.* **2018**, *184*, 598−608.
(11) Wu, Z.; Zhang, X.; Wu, M. Mitigating construction dust pollution: State of the art and the way forward. *J. Clean Prod.* **2016**, *112*, 1658−1666.
(12) Yang, J.; Fan, X.; Zhang, H.; Zheng, W.; Ye, T. A review on characteristics and mitigation strategies of indoor air quality in underground subway stations. *Sci. Total Environ.* **2023**, *869*, 161781.
(13) Chen, X.; Guo, C.; Song, J.; Wang, X.; Cheng, J. Occupational health risk assessment based on actual dust exposure in a tunnel construction adopting roadheader in Chongqing, China. *Build Environ.* **2019**, *165*, 106415.
(14) Yan, H.; Ding, G.; Feng, K.; Zhang, L.; Li, H.; Wang, Y.; Wu, T. Systematic evaluation framework and empirical study of the impacts of building construction dust on the surrounding environment. *J. Clean Prod.* **2020**, *275*, 122767.
(15) Lioy, P. J.; Freeman, N. C. G.; Millette, J. R. Dust: a metric for use in residential and building exposure assessment and source characterization. *Environ. Health Perspect.* **2002**, *110* (10), 969−983.
(16) Pokonova, Y. V. Preparation and characterization of anion exchangers from petroleum asphaltites. *Solid Fuel Chem.* **2011**, *45* (4), 275−280.
(17) Shi, G.; Qi, J.; Wang, Y.; Liu, S. Experimental study on the prevention of coal mine dust with biological dust suppressant. *Powder Techno.* **2021**, *391*, 162−172.
(18) Amato, F.; Querol, X.; Johansson, C.; Nagl, C.; Alastuey, A. A review on the effectiveness of street sweeping, washing and dust suppressants as urban PM control methods. *Sci. Total Environ.* **2010**, *408* (16), 3070−3084.
(19) Parsakhoo, A.; Hosseini, S. A.; Lotfalian, M.; Mohammadi, J.; Salarijazi, M. Effects of molasses, polyacrylamide andbentonite on dust control in forest roads. *Journal of Forest Science* **2020**, *66* (5), 218−225.
(20) Orszulik, E.; Dudek, W. Testing Dust Control Preparation with Respect to Mine EmployeeExposure to Inhalling Chemical Agents. *J. Sustain Min.* **2013**, *12* (4), 14−17.
(21) Xu, G.; Chen, Y.; Eksteen, J.; Xu, J. Surfactant-aided coal dust suppression: A review of evaluation methods and influencing factors. *Sci. Total Environ.* **2018**, *639*, 1060−1076.
(22) Medeiros, M. A.; Leite, C.; Lago, R. M. Use of glycerol by-product of biodiesel to produce anefficient dust suppressant. *Chem. Eng. J.* **2012**, *180*, 364−369.
(23) Tsai, Y. T.; Yang, Y.; Huang, H. C.; Shu, C. M. Inhibitory effects of three chemical dust suppressants on nitrocellulose dust cloud explosion. *AIChE J.* **2020**, *66* (5), 16888.
(24) Dong, H.; Yu, H.; Xu, R.; Cheng, W.; Ye, Y.; Xie, S.; Zhao, J.; Cheng, Y. Review and prospects of mining chemical dust suppressant: Classification and mechanisms. *Environ. Sci. Pollut Res. Int.* **2023**, *30* (1), 18−35.
(25) Amato, F.; Querol, X.; Johansson, C.; Nagl, C.; Alastuey, A. A review on the effectiveness of street sweeping, washing and dust suppressants as urban PM control methods. *Sci. Total Environ.* **2010**, *408* (16), 3070−3084.
(26) Zhang, Q.; Fan, L.; Wang, H.; Han, H.; Zhu, Z.; Zhao, X.; Wang, Y. A review of physical and chemical methods to improve the performance of water for dust reduction. *Process Saf Environ. Prot.* **2022**, *166*, 86−98.
(27) Casas, J. A.; Mohedano, A. F.; García-Ochoa, F. Viscosity of guar gum and xanthan/guar gum mixture solutions. *J. Sci. Food Agric.* **2000**, *80* (12), 1722−1727.
(28) Mudgil, D.; Barak, S.; Khatkar, B. S. X-ray diffraction, IR spectroscopy and thermal characterization of partially hydrolyzed guar gum. *Int. J. Biol. Macromol.* **2012**, *50* (4), 1035−1039.
(29) Khouryieh, H.A.; Herald, T.J.; Aramouni, F.; Alavi, S. Intrinsic viscosity and viscoelastic properties of xanthan/guar mixtures in dilute solutions: Effect of salt concentration on the polymer interactions. *Food Res. Int.* **2007**, *40* (7), 883−893.
(30) Ribotta, P.D.; Perez, G.T.; Leon, A.E.; Anon, M.C. Effect of emulsifier and guar gum on micro structural, rheological and baking performance of frozen bread dough. *Food hydro.* **2004**, *18* (2), 305−313.
(31) Taunk, K.; Behari, K. Graft copolymerization of acrylic acid onto guar gum. *J. Appl. Polym. Sci.* **2000**, *77* (1), 39−44.
(32) George, M.; Abraham, T. E. pH sensitive alginate-guar gum hydrogel for the controlled delivery of protein drugs. *Int. J. Pharm.* **2007**, *335* (1), 123−129.
(33) Wu, M.; Hu, X.; Zhang, Q.; Zhao, Y.; Sun, J.; Cheng, W.; Fan, Y.; Zhu, S.; Lu, W.; Song, C. Preparation and performance evaluation of environment-friendly biological dust suppressant[J]. Journal of Cleaner Production. *J. Clean Prod.* **2020**, *273*, 123162.


https://doi.org/10.1021/acsomega.3c07734
*ACS Omega* 2024, 9, 3746−3757

(34) Zhang, H.; Nie, W.; Wang, H.; Bao, Q.; Jin, H.; Liu, Y. Preparation and experimental dust suppression performance characterization of a novel guar gum-modification-based environmentally-friendly degradable dust suppressant. *Powder Techno.* **2018**, *339*, 314−325.
(35) Hongbo, T.; Yanping, L.; Min, S. Preparation and property of crosslinking guar gum. *J. Appl. Polym. Sci.* **2012**, *44* (3), 211−216.



https://doi.org/10.1021/acsomega.3c07734
*ACS Omega* 2024, 9, 3746−3757